

pubs.acs.org/JPCA Article

Low-Temperature Water Uptake of Individual Marine and Biologically Relevant Atmospheric Particles Using Micro-Raman Spectroscopy

Published as part of The Journal of Physical Chemistry virtual special issue "125 Years of The Journal of Physical Chemistry".

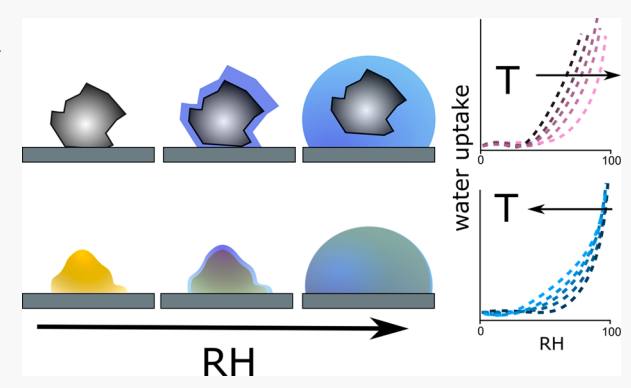
Liora E. Mael, Heidi L. Busse, Gordon Peiker, and Vicki H. Grassian*



ACCESS

Metrics & More

ABSTRACT: The interaction of water vapor and the water uptake behavior of atmospheric particles are often investigated as a function of relative humidity (0-100% RH) at ambient temperature. However, lower temperature studies are important to understand how atmospheric particles nucleate ice through various mechanisms including immersion freezing. Immersion freezing requires the formation of a condensed water droplet at lower temperatures prior to freezing. To better understand low-temperature water uptake behavior of marine and biologically relevant atmospheric particles, we have investigated water uptake of single atmospheric particles using a micro-Raman spectrometer coupled to an environmental cell for measurements at lower temperatures and as a function of relative humidity. These particles include sodium chloride, sucrose, Snomax,



Article Recommendations

lipopolysaccharide, and laminarin. Particles range in size from 2 to 3 μ m in diameter and can be monitored by using optical microscopy and Raman spectroscopy as a function of relative humidity at temperatures between 253 and 298 K. From the Raman spectra collected, we can determine a Raman growth factor defined as an increase in the intensity of the O–H stretch as a measure of the integrated water content of a particle compared to the dry particle. These data show that for lipopolysaccharide, laminarin, and Snomax, unlike simple saccharides such as sucrose and other soluble organics, as temperature decreases, water uptake begins at lower relative humidity and does not follow a solubility temperature dependence. This suggests that at lower temperatures the particles are adsorbing water on the surface rather than dissolving and absorbing water. Furthermore, repeated water uptake cycles cause a change in the morphology of some of these particles, which is shown to promote water uptake at lower relative humidity. These results give new insights into water uptake of these different marine and biologically relevant particles at low temperature at subsaturation relative humidity prior to droplet formation and immersion freezing.

INTRODUCTION

Mixed-phase clouds are important to the hydrological cycle and radiative budget of the earth. ^{1–3} They have been observed and measured year-round across the globe, but their complex composition of supercooled water and ice crystals makes them difficult to model. ⁴ The formation, composition, size, precipitation, and density of mixed-phase clouds and thus their effect on the hydrological cycle and radiative balance are all affected by aerosol composition. ¹ A small but important subset of these aerosols act as ice nucleating particles (INPs) which provide a heterogeneous substrate to glaciate clouds. INPs induce ice formation before water homogeneously freezes in the atmosphere around 235 K, contributing to ice and mixed-phase cloud formation. ^{5–7} The predominate pathway for the formation of ice in mixed-phase clouds is

immersion freezing, in which an INP takes up water to form a supercooled droplet prior to freezing. Though ice nucleation has been extensively studied, there is ongoing work to identify the chemical and physical properties that control the activity of marine and biologically relevant INP. Mixed-phase clouds are particularly impactful in the southern hemisphere in remote marine environments, where sea spray aerosol (SSA) derived INPs are the greatest contributors to these clouds. Let 12-14

Received: September 11, 2021 Revised: October 8, 2021



The defining feature of immersion mode freezing is the inclusion of INPs in a droplet prior to freezing. Therefore, the water uptake behavior of an aerosol as a function of temperature determines the ice nucleating pathway of an INP in the atmosphere, ultimately impacting cloud formation, the hydrological cycle, and the radiative budget. Herein we probe the temperature dependence of water uptake of different micrometer-sized particles to elucidate how marine and biologically relevant particles interact with water vapor under subsaturation conditions. Exposure to increasing relative humidity (RH) for inorganic particles, for instance sodium chloride, can lead to phase transitions such as deliquescence at a distinct, thermodynamically determined RH. 15-17 This transition from a crystalline particle to a droplet occurs at a substance specific deliquescence relative humidity (DRH) and is followed by the rapid, continuous growth of the droplet. 15,18,19 In contrast, organic and biologically relevant particles can grow gradually, taking up water even at low RH. 16,19,20 Estillore et al. suggest that one possible reason for the continuous water uptake of these organic particles is the presence of physical defects within the particles. 16 These cracks, pores, and grainlines on the surface of particles may play a role and promote water adsorption and absorption at lower RH. Taken together, these processes define the water uptake of these different types of atmospherically relevant particles.

The water uptake and deliquescence of both organic and inorganic single particles have been studied at ambient temperatures across a broad range of instruments, giving insights into chemical and physical properties of these different systems. 17,20–28 However, the majority of these measurements are made at ambient temperature, at or near 298 K. Clearly, lower temperature measurements are important as this is where mixed-phase and ice cloud temperature regimes are relevant, that is, the temperature range where an aerosol may act as an INP. Previous temperature-dependent studies have focused on the deliquescence of inorganic salts and water uptake of small organics. This includes work from Martin and Gysel et al. that show minimal variation in deliquescence with temperature for NaCl and sulfate salts, respectively. 13,15 Guo et al. report an increase in DRH values of nitrate salts with decreased temperature consistent with the temperature dependence that can be approximated from the Clausius-Clapeyron equation (as related to solubility) but minimal temperature dependence on the chloride salts were measured.²⁹ Similarly, the results of low-temperature organic water uptake vary. Zamora et al. have shown little to no temperature dependence of saccharides, mono/dicarboxylic acids, and humic-like substances between 273 and 303 K.30 Conversely, Baustian et al.²² measure a clear negative temperature dependence of sucrose, glucose, and citric acid (used as small organic secondary organic aerosol (SOA) proxies) between 200 and 273 K, which can be related to the solubility of these SOA proxies, similar to what was observed for nitrate salts.²⁹ Ganbavale et al. measured the water activity temperature dependence of a range of soluble organic systems also between 200 and 273 K using multiple techniques including an electrodynamic balance and differential scanning calorimetry, finding the behavior of these organic systems different from the predicted temperature dependence, and indicated a need for further measurements at low temperatures to improve predictions of the ice nucleation ability of mixed aqueous systems.³¹

The water uptake and deliquescence of supermicrometer particles have been measured by multiple techniques, ranging from suspended particles (electrodynamic balance, hygroscopic tandem differential mobility analyzer) to single particles on substrates (Raman, atomic force microscopy, atomic force microscopy-infrared spectroscopy).²⁶ In this study Raman spectroscopy is used as it can detect the vibrational signature of condensed water molecules.^{32,33} The broad spectral region of interest between 3000 and 3800 cm⁻¹ is associated with the O-H stretching vibration of water. We monitored this region to investigate a range of micrometer-sized particles that include NaCl, sucrose, lipopolysaccharide (LPS), laminarin, and Snomax. For these different particles, there is a range of immersion freezing ice nucleation onset temperatures. NaCl was chosen as a purely inorganic salt representative and control as it is well characterized across a range of instruments and temperatures. Additionally, NaCl does not freeze until very low temperatures ca. 215 K, outside of the temperature range reached by the environmental cell used in this experiment (vide infra). 15,20,34,35 Sucrose was chosen as a simple, wellcharacterized saccharide whose water uptake across a broad range of temperatures has been previously studied. 22,31,36,37 Sucrose, similar to NaCl, is a poor INP, previously shown to freeze between 205 and 235 K.²² In addition, saccharides are known to comprise a large portion of the dissolved organic carbon in the ocean.³⁸ LPS and laminarin were chosen because they have both been identified as marine relevant biological particles. LPS has a moderate immersion ice nucleation ability $(249.4 \pm 0.7 \text{ K})$ and is composed of polysaccharide chains found on the surfaces of Gram-negative bacteria. 11,35 Previous work from Maeda et al. has determined LPS to be an indicator of biomass blooms which have been observed in the South China Sea and Pacific Ocean.³⁹ Laminarin is a complex sugar produced during cell wall degradation that has poor ice nucleating abilities, measured here to freeze within the same range as water in our studies $(246.6 \pm 1.1 \text{ K})^{16}$ Additionally, laminarin has been found to make up a significant fraction of particulate organic matter found in ocean waters and to play a significant role in the marine carbon cycle and ocean carbon sequestration.⁴⁰ Finally, Snomax, a commercial product derived from proteins in the bacteria Pseudomonas syringae, was chosen as an excellent ice nucleating particle (268.2 ± 0.8 K). 35,41 In this work, the Raman spectra associated with these different micrometer-sized particles were characterized as a function of relative humidity at several temperatures within the range of ca. 250–300 K to further reveal potential connections of subsaturation water uptake and ice nucleating behavior. The overall goal of this study is to gain an improved understanding of the chemical and physical properties of marine and biologically relevant particles that contribute to INP and mixed-phase clouds, and thus contribute to reducing uncertainties in global and regional climate models.^{42,43}

■ EXPERIMENTAL METHODS

Materials, Chemicals, and Sample Preparation. All chemicals were purchased directly from the manufacturers and used without further sterilization or purification and included sodium chloride (NaCl, ≥99% Fisher Scientific), sucrose (≥99%, Sigma-Aldrich), *Pseudomonas syringae* (Snomax, York Snow Inc.), lipopolysaccharide (LPS, L4130, extracted from *E. coli* 0111:B4, purified by trichloroacetic acid extraction, Sigma-Aldrich), and laminarin (Alfa Aesar). Aqueous solutions were prepared with Milli-Q ultrapure water. Samples were

generated by passing aqueous solutions of compounds listed above first through an atomizer (TSI Inc., Model 3062) and then two silica diffusion driers (RH < 5%) before they were collected on hydrophobically coated (Rain-X) quartz substrates (Ted Pella Inc., part no 16001-1).

Water Uptake and Ice Nucleation Measurements. A Raman microscope with a 532 nm laser (Horiba, LabRam HR Evolution) combined with an environmental cell (Linkam, LTS 120) was used to study water uptake and ice nucleation as described in Mael et al. 35 Substrates with different individual particle samples were placed inside the environmental cell to equilibrate at 298 K for ~20 min under dry N₂, where the relative humidity (RH) was monitored with a hygrometer (Buck Research Instruments, CR-4). The temperature of the cell was then set for a specific temperature, and an additional 20 min was given for the system to stabilize to the temperature of interest. After this, a mixture of dry and humidified N₂ was introduced to the cell to increase RH to ~10% RH followed by an additional 15 min calibration period following the stabilization of the RH. A Raman spectrum was then taken between 2600 and 4000 cm⁻¹ with five exposures of seven seconds each. This was continued, increasing the ratio of humidified N₂ to dry N₂ flowing into the cell systematically, until an RH of ca. 100% was reached. Following water uptake measurements, ice nucleation measurements were made as described in Mael et al.³⁵

Following each experiment, the cell temperature was returned to 298 K and the ratio of humidified to dry N₂ flowing into the cell was decreased. Once the hygrometer had reached equilibrium, the particles and environmental cell were dried out for an additional 10 min. Subsequent water uptake measurements were performed on the same particle at different temperatures. To investigate potential phase changes or templating that may occur from repeated measurements on the same particle, multiple temperature "cycles" were probed in at least triplicate. The three temperature cycles were (1) 298 K \rightarrow 283 K \rightarrow 273 K \rightarrow 263 K \rightarrow 253 K, (2) 253 K \rightarrow 263 K \rightarrow 273 K \rightarrow 283 K \rightarrow 298 K, and (3) 273 K \rightarrow 253 K \rightarrow 283 K \rightarrow 298 K \rightarrow 263 K. With each new temperature cycle, a new particle was interrogated. For Snomax, because of its low ice nucleation onset temperature, measurements were only collected to a low temperature of 273 K.

RESULTS AND DISCUSSION

For these water uptake measurements, a deposited dry particle was subjected to increasing RH within the environmental cell at each temperature. The particle morphology was observed with an optical microscope. As can be seen in Figure 1, there is a transition of the initial, dry-deposited particle to a dark circle with a characteristic white center, indicative of a liquid droplet. This white dot at the center of the liquid particles is due to illumination by a white light source above the sample used for imaging. Additionally, this transition was monitored with Raman spectroscopy by observing growth in the band associated with the O-H stretching motion, $\nu(OH)$, from 3000 to 3800 cm⁻¹ (as seen in Figure 2). Following one cycle of increasing and decreasing RH, NaCl and Snomax visually return to their original dry-deposited structure. Similarly, sucrose particles returned to their initial dry deposited morphology following several cycles, although the initial "dry" particles appear droplet-like but much smaller. The impact of these increasing and decreasing RH cycles is different for laminarin-containing particles. Following the first

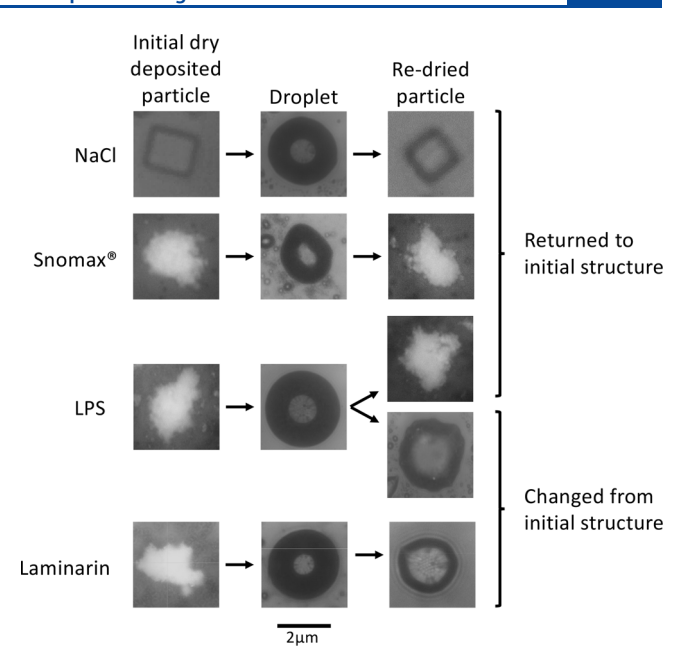


Figure 1. Images corresponding to the morphologies of particles at different stages of increasing and decreasing RH. The left column shows images of the initial dry deposited particle. The middle column shows the particles after droplets have formed at 100% RH. The right column shows the particle morphology after being re-dried.

increase in RH, upon drying, the particle adopts a rounded, more amorphous morphology, different from the dry-deposited initial structure. For each subsequent water uptake and loss cycle, laminarin particles returned to this amorphous state rather than the initial dry-deposited structure as seen with NaCl, sucrose and Snomax. In the case of LPS particles, these particles predominantly returned to their original drydeposited morphologies following decreasing RH, but in fact a very small fraction (<5%) of the particles show a morphology change to a more rounded amorphous shape, as shown in Figure 1. Following an additional RH cycle, amorphous LPS particles return to their original, dry-deposited morphologies. Interestingly, these different morphologies did not impact the particles water uptake behavior (Figure 2). Although these morphology changes are not completely understood, LPS has been observed to change its morphology due to the coordination of different cations in its structure.⁴⁴

In addition to monitoring the optical images, the details of water interaction with these particles are monitored by integration of the O–H Raman stretching band (between 3000 and 3800 cm $^{-1}$). For NaCl (Figure 2a), the spectra as a function of RH can clearly be clearly seen to increase at the deliquescence relative humidity (DRH) of 75 \pm 2%, in agreement with literature. This transition from solid to liquid is followed by the rapid, continuous growth of the particle as seen in the sustained increase in Raman intensity at RH values above the DRH. For sucrose, Snomax, laminarin, and LPS, there is no distinct transition from solid to liquid, but instead there is a gradual increase in intensity of the O–H stretching region across a range of RH values. This can initially be seen as an increase in Raman intensity at low- to mid-RH and more rapidly at higher RH values (Figure 2b–e).

For water uptake measurements across a temperature range, the same particle is probed repeatedly through increasing and decreasing relative humidities at each temperature. The same

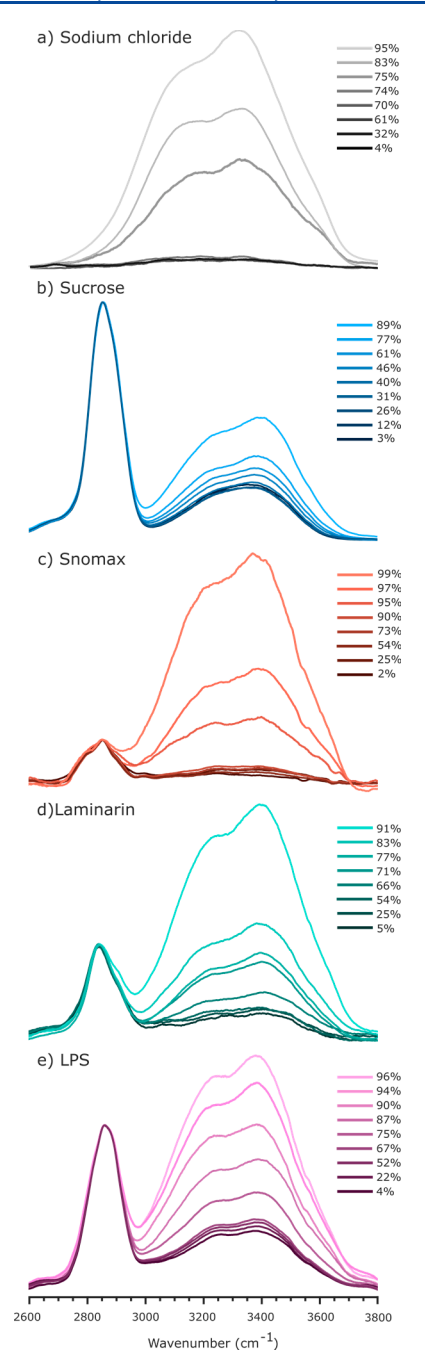


Figure 2. Raman spectra taken at 298 K for (a) sodium chloride (black), (b) sucrose (blue), (c) Snomax (orange), (d) laminarin (teal), and (e) LPS (purple) as a function of %RH from 2 to 96 %RH. These spectra have all been baseline corrected and normalized to the highest intensity peak in the 2800 to 3800 cm⁻¹ region.

particle for NaCl, sucrose, LPS, and Snomax showed no change in water uptake behavior between cycles. Additionally, when different morphologies of LPS particles were observed, the water uptake behavior was also the same. However, for laminarin, there was a significant difference in water uptake between the initial dry deposited particle and the particle following the first increasing/decreasing RH cycle. Subsequent cycles show no significant variation in water uptake when the particle was present as a rounded amorphous morphology. Changes in the O–H stretching region as a f(RH) were used to create plots of a Raman growth factor as a function of

temperature for each of these different micrometer-sized particles as shown in Figures 3 and 4. The Raman growth factor (GF) has been previously defined as²⁰

Raman GF =
$$A/A_0$$
 (1)

in which A is the integrated area of the O–H stretching region between 3000 and 3800 cm⁻¹ of the particle and A_0 is the integrated area at the lowest RH measured. The Raman growth factors for these different particles as a f(RH) were fit with a parametrized function modified (Figure 3) from Dick et al. 47

$$GF = \left[1 + (a + ba_{w} + ca_{w}^{2}) \frac{a_{w}}{1 - a_{w}}\right]^{1/3}$$
 (2)

where a, b, and c are adjustable parameters and a_w is the water activity, equal to RH/100.¹⁶ The parameters for the organics (a, b, and c) are given in Table 3. This GF fit was developed for use with tandem differential mobility analyzer (TDMA) RHdependent particle growth measurements. The parametrized fit function was applied to our Raman GF data as measurements from Laskina et al. have shown comparable GF behavior is observed between the humidified tandem differential mobility analyzer (HTDMA) and Raman GF measurements for single particles or inorganic salts and mixed organic and inorganic systems.²⁰ It should be noted that while the GF curves are comparable, the absolute GF values are not. As such, these Raman GF data can be compared at different temperatures for a single particle. The X^2 values associated with the fits for the different particles across the temperature range can be found in Table 3 and were used to confirm the "goodness" of the fit. While the X^2 values reported are small, indicating a good fit, the error associated with the individual parameters is fairly large. One reason may be that the GF of the lower RH region at temperatures below 298 K show a small local maximum before the initial water uptake begins. This is a product of the fit rather than an indication of a trend in the data, as these low RH GF values do not deviate significantly from the initial values.

Figure 4 shows the dry deposited water uptake behavior of laminarin as compared to the amorphous particles in terms of the Raman spectra, optical images, and the calculated Raman GF values. Beyond the physical changes in the samples between the dry deposited and the amorphous particles following an increasing/decreasing RH cycle, there is a difference in the water uptake behavior of laminarin, though not LPS, which can also be seen in Figure 4. Water uptake onset, highlighted in blue, begins 5-30% higher when the particle is dry deposited (Figure 4a,c,e) than when it is amorphous (Figure 4b,d,f). For these particles where there is no clear DRH as there is for a pure inorganic salt (like NaCl), we define water uptake to begin when the calculated Raman GF is significantly different from several values taken at the lower RH, (as determined by a one-tailed t test, $\alpha = 0.025$). The spectra highlighted correspond to the first RH for these higher Raman GF values.

Previous work by Baustian et al. has shown variation in morphology associated with changes in the Raman spectrum. The particles measured in this work do not show any spectral differences between the dry deposited and amorphous particles, indicating that this difference in laminarin morphology may be due to initially drying the suspended atomized particles via diffusion dryers versus drying the deposited particles in the environmental cell following increasing/

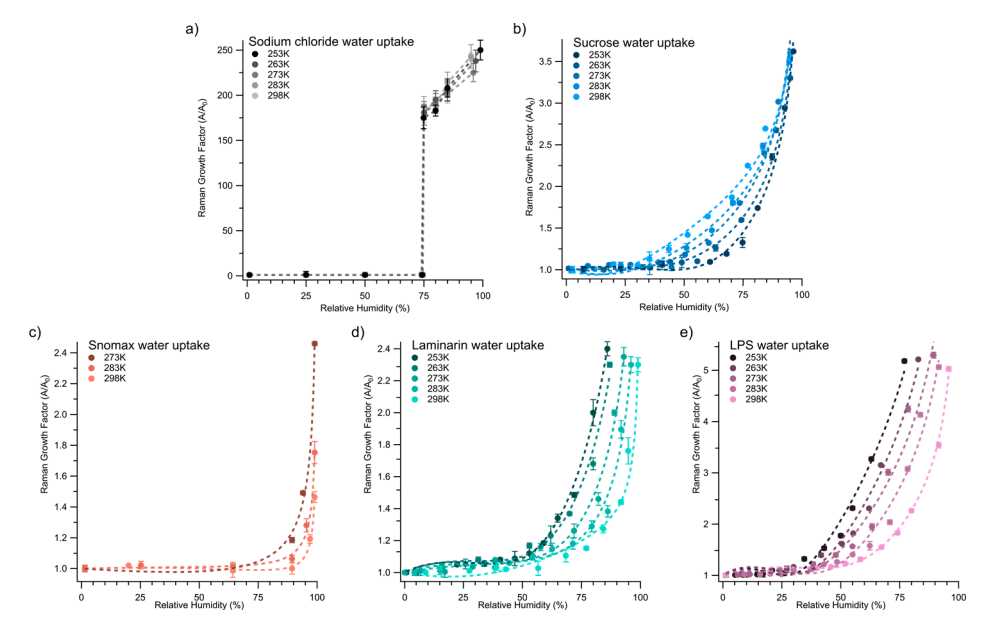


Figure 3. Temperature-dependent water uptake curves, as measured by a Raman growth factor (eq 1), as a f(RH). Water uptake curves between low temperature (darker data points) and higher temperatures (lighter data points) for (a) NaCl (black), (b) sucrose (blue), (c) Snomax (orange), (d) laminarin, amorphous (teal), and (e) LPS (purple). Lines represent fits to the data using eq 2 (see text for further details). Notably, pure NaCl shows no temperature dependence, sucrose shows water uptake occurs at lower %RH with increasing temperature, whereas the better INP, Snomax, laminarin, and LPS all show water uptake occurs at lower relative humidity with decreasing temperature.

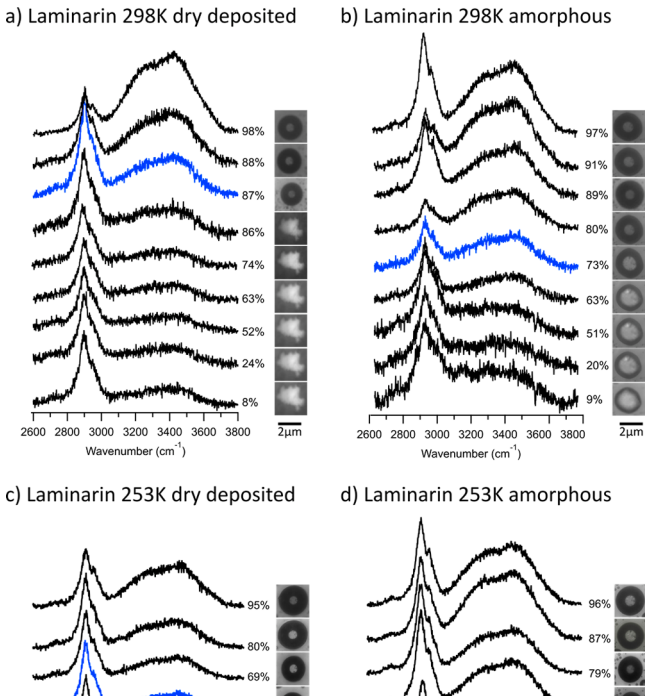
decreasing RH. This difference in dry deposited and amorphous particle morphology water uptake may be due to hysteresis effects where the addition of water to an already solubilized sample requires less energy and occurs at lower RH than adding water to a crystalline, or in this case, a dry deposited sample of the same material at the same temperature.¹⁹ The water uptake curves for laminarin in Figure 3c report the water uptake of the amorphous particles, which following the initial increasing/decreasing RH cycle did not deviate significantly between repeated cycles. Notably, this difference in water uptake behavior does not affect the immersion freezing behavior of either LPS or laminarin. Table 1 compiles IN onset temperatures measured for these different particles. These IN onset values agree with earlier measurements made (see ref 33 for full details). As reported in Table 1, there is no statistical difference between the dry deposited and amorphous particle freezing temperatures. This is not to say that the different morphologies (crystalline vs glassy or amorphous) would not affect depositional freezing at lower temperatures where a particle does not form a droplet prior to freezing.

An analysis of the value of the initial water uptake RH for sucrose, Snomax, LPS, and laminarin at different temperatures is given in Table 2. These values were determined to be statistically significant relative to the values at lower RH (as determined by a one-tailed t test, $\alpha = 0.025$). In accordance with the literature, sucrose shows an increase in the RH for initial water uptake with decreasing temperature. ^{22,31,36,37} Conversely, Snomax, LPS, and laminarin show the opposite correlation between the initial RH and temperature, i.e., where water uptake begins at higher RH with increasing temperatures. Additionally, the water uptake onset RH is consistently higher for Snomax than for laminarin and LPS (Snomax > laminarin > LPS). Snomax only shows water uptake above 75% RH, significantly higher than any of the other organic systems investigated. This is most likely due to the insolubility of

Snomax and is consistent with other measurements of the behavior of proteins as a function of RH. LPS, which has a saccharide component, and laminarin, which is a highly branched polysaccharide, are fairly insoluble and show very similar water uptake behavior. Interestingly, these differences in the onset relative humidity have a similar trend with ice nucleation onset temperatures for laminarin, LPS, and Snomax. Laminarin and LPS, which nucleate ice ca. 248 K, take up water beginning at a much lower RH (between 44% and 73% RH) than Snomax, which has a much warmer ice nucleation onset temperature (268 K) and does not take up water until above 75% RH.

While the water uptake as a function of temperature follows a similar trend for Snomax, laminarin, and LPS, it differs from the water uptake of the more soluble saccharide, sucrose, and the pure inorganic NaCl. For both NaCl and sucrose, our measurements follow previously reported data. Therefore, measurements of more complex organic and biological species showing quite different behavior is not due to any artifact of the experimental technique but instead due to very different temperature-dependent behavior.

Raman GF values for sucrose, LPS, laminarin, and Snomax can be calculated by using eq 2 at $85 \pm 2\%$ RH, as shown in Table 4. As discussed earlier, Raman GF values can be used to assess trends in water uptake behavior across different temperatures of the same particle type. The measured Raman GF values for sucrose decrease with decreasing temperature, in accordance with the trends seen in initial water uptake behavior measured here experimentally, the literature, and as predicted by the Clausius–Clapeyron equation. ^{21,44–46} Unlike sucrose, Snomax, LPS, and laminarin show a clear positive trend with decreasing temperature, indicating that at the same RH, particles had more water associated with them at lower temperatures. The opposing trends in water uptake behavior for sucrose versus other organic particles at a fixed relative humidity further support



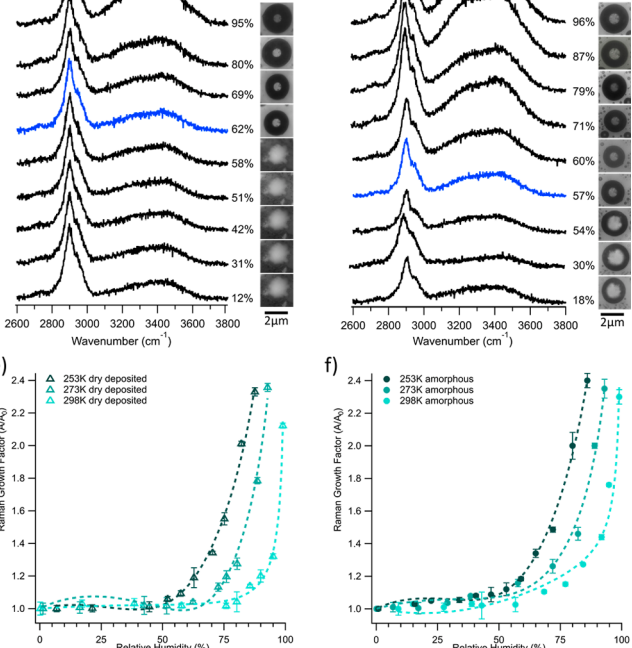


Figure 4. Raman spectra of laminarin at 298 K with increasing relative humidity for a (a) dry deposited particle and (b) amorphous particle and at 253 K for a (c) dry deposited and (d) amorphous particles. The corresponding Raman growth factor curves between low temperature (darker data points) and higher temperatures (lighter data points) for (e) the dry deposited laminarin (open triangle markers) and (f) amorphous laminarin (closed circles) are shown below. The blue spectra are highlighted for each of these morphologies to show the relative humidity where water uptake begins and, for the dried deposited particle, where the morphology changes.

that the water uptake mechanisms are different between the two types of organics.

Based on previous work, ^{22,30,49} we would expect water uptake to be suppressed at lower temperatures, with the onset of water uptake occurring at higher RHs. This is what is observed for sucrose which follows the temperature-dependent solubility approximated by the Clausius-Claperyon equation. ^{29,50,51} Laminarin, LPS and Snomax all show an opposite temperature dependence. This indicates that particles

Table 1. Summary of Experimental Measurements of Immersion Freezing Onset Temperatures of Micrometer-Sized Droplets of Water, NaCl, Sucrose, Laminarin, LPS, and Snomax

	ice nucleation onset temp (K)
water	246.3 ± 1.0
NaCl	<246
sucrose	<246
laminarin (amorphous)	246.6 ± 1.1
laminarin (dry deposited)	246.8 ± 0.9
LPS (amorphous)	249.9 ± 1.1
LPS (dry deposited)	249.5 ± 0.8
Snomax	268.1 ± 0.9

Table 2. Summary of Water Uptake Onset Relative Humidities (as %RH) at Different Temperatures for Sucrose, LPS, Laminarin, and Snomax between 298 and 253 K^a

temp (K)	sucrose	Snomax	larminarin	LPS
298	37 ± 2	97 ± 3	73 ± 2	69 ± 3
283	45 ± 3	96 ± 2	71 ± 3	60 ± 2
273	50 ± 3	89 ± 4	67 ± 3	55 ± 2
263	58 ± 2		60 ± 2	48 ± 3
253	67 ± 2		57 ± 3	44 ± 3

 $^a\mathrm{Values}$ are not available for Snomax below its freezing temperature of 269 K.

Table 3. Summary of the GF Fitting Parameter Values Used in Eq 2 of Sucrose, LPS, Laminarin (Amorphous and Dry Deposited), and Snomax across All Temperatures Measured

temp (K)	а	Ь	с	χ^2	
sucrose					
298	-2.8 ± 1.2	14.1 ± 3.9	-8.9 ± 2.9	0.08	
283	-2.0 ± 1.6	7.6 ± 4.9	-3.0 ± 3.5	0.05	
273	-0.4 ± 1.2	0.9 ± 3.9	2.5 ± 2.9	0.08	
263	0.3 ± 1.2	-1.9 ± 3.7	3.9 ± 2.7	0.06	
253	1.4 ± 1.5	-6.4 ± 4.2	7.2 ± 2.8	0.08	
		Snomax			
298	0.1 ± 0.3	-0.5 ± 0.7	0.3 ± 0.4	0.001	
283	0.1 ± 0.4	-0.2 ± 0.9	0.2 ± 0.5	0.003	
273	-0.3 ± 1.1	0.5 ± 2.6	-0.0 ± 1.4	0.006	
	lamir	narin (amorphous)		
298	-0.8 ± 0.5	2.8 ± 1.4	-1.9 ± 0.8	0.05	
283	0.8 ± 0.6	-2.0 ± 1.7	1.7 ± 1.1	0.02	
273	1.3 ± 0.6	-4.1 ± 1.9	3.9 ± 1.3	0.01	
263	2.0 ± 0.8	-7.0 ± 2.5	7.5 ± 2.0	0.01	
253	2.2 ± 0.4	-8.9 ± 1.6	10.3 ± 1.3	0.009	
laminarin (dry deposited)					
298	0.3 ± 0.2	-0.7 ± 0.6	0.5 ± 0.3	0.005	
273	2.3 ± 0.7	-8.1 ± 2.0	7.0 ± 1.4	0.01	
253	1.1 ± 0.6	-5.6 ± 2.1	7.3 ± 1.6	0.01	
LPS					
298	-0.3 ± -0.2	1.7 ± 0.7	-1.1 ± 0.4	0.003	
283	0.4 ± 0.2	-1.1 ± 0.9	2.2 ± 0.7	0.003	
273	1.1 ± 0.5	-4.5 ± 1.8	6.7 ± 1.5	0.005	
263	0.7 ± 0.5	-2.4 ± 1.8	5.6 ± 1.6	0.003	
253	0.8 ± 0.5	-3.0 ± 2.2	7.9 ± 2.1	0.002	

composed of laminarin, LPS or Snomax are not simply dissolving or absorbing water as RH is increased in the same manner as a soluble saccharide such as sucrose. Instead, these

Table 4. Relative Raman Growth Factors at RH = $85 \pm 2\%$ of Sucrose, Snomax, Laminarin, and LPS at Different Temperatures^a

temp (K)	sucrose	Snomax	laminarin	LPS
298	2.55 ± 0.2	0.82 ± 0.2	1.30 ± 0.2	1.44 ± 0.3
283	2.41 ± 0.2	1.1 ± 0.2	1.42 ± 0.2	1.91 ± 0.3
273	2.37 ± 0.2	1.4 ± 0.2	1.66 ± 0.2	2.35 ± 0.3
263	2.11 ± 0.2	_b	2.10 ± 0.2	2.54 ± 0.3
253	1.96 + 0.2	_ <i>b</i>	2.34 + 0.2	2.86 + 0.3

^aThe error reported is the largest error measured from the Raman GF plots in Figure 3. ^bBelow the freezing temperature.

more complex macromolecules, which behave as better INP, are insoluble and show a different temperature dependence that provides a surface for water adsorption within small nanoscale pores and on the particle surface. It is important to note that although we are not seeing water absorption by these particles, we do see these particles preferentially adsorbing water on the surface at higher RH values, to form droplets, as compared to the substrate alone. It has been shown previously that thin films may begin to form on NaCl particle surfaces prior to deliquescence. Here we suggest that on the surface of these porous macromolecules thin films of water are forming and these films can become microscopically thick.

CONCLUSIONS

In this study, we investigated the temperature dependence of the water uptake of a range of different micrometer-sized particles from pure salt to simple saccharides to more complex organics and biological macromolecules. The results show a decrease in initial water uptake RH with decreased temperature for these larger more complex macromolecules. This temperature dependence supports the fact that these macromolecules are insoluble, and the temperature dependence is not related to solubility as it is for a simple soluble saccharide such as sucrose. The data show that while droplets are forming, it is most likely that the particles of LPS, laminarin, and Snomax are inclusions within the droplet rather than dissolved. Additionally, we show a difference in water uptake behavior between dry deposited and amorphous particles, though these different morphologies do not yield a change in the immersion freezing behavior. Overall, this work provides insights into the water uptake of INPs in the atmosphere over a range of temperatures and the behavior of complex organic and biological particles known to be important in ice nucleation and mixed-phase cloud formation.

AUTHOR INFORMATION

Corresponding Author

Vicki H. Grassian — Department of Chemistry & Biochemistry, University of California, San Diego, La Jolla, California 92037, United States; orcid.org/0000-0001-5052-0045; Email: vhgrassian@ucsd.edu

Authors

Liora E. Mael – Department of Chemistry & Biochemistry, University of California, San Diego, La Jolla, California 92037, United States

Heidi L. Busse – Department of Chemistry & Biochemistry, University of California, San Diego, La Jolla, California 92037, United States Gordon Peiker – Department of Chemistry & Biochemistry, University of California, San Diego, La Jolla, California 92037, United States

Complete contact information is available at: https://pubs.acs.org/10.1021/acs.jpca.1c08037

Notes

The authors declare no competing financial interest.

ACKNOWLEDGMENTS

This work was funded by the National Science Foundation (NSF) through the NSF Center for Aerosol Impacts on the Chemistry of the Environment (NSF-CAICE), a Center for Chemical Innovation (CHE-1801971), and the Nation Science Foundation Graduate Research Fellowship Program (DGE-1650112).

REFERENCES

- (1) Lohmann, U.; Feichter, J. Global Indirect Aerosol Effects: A Review. *Atmos. Chem. Phys.* **2005**, *5* (3), 715–737.
- (2) Clouds and Aerosols. In Climate Change 2013 The Physical Science Basis: Working Group I Contribution to the Fifth Assessment Report of the Intergovernmental Panel on Climate Change; Intergovernmental Panel on Climate Change, Ed.; Cambridge University Press: Cambridge, 2014; pp 571–658.
- (3) DeMott, P. J.; Mason, R. H.; McCluskey, C. S.; Hill, T. C. J.; Perkins, R. J.; Desyaterik, Y.; Bertram, A. K.; Trueblood, J. V.; Grassian, V. H.; Qiu, Y.; et al. Ice Nucleation by Particles Containing Long-Chain Fatty Acids of Relevance to Freezing by Sea Spray Aerosols. *Environ. Sci. Process. Impacts* **2018**, 20 (11), 1559–1569.
- (4) Shupe, M. D.; Daniel, J. S.; de Boer, G.; Eloranta, E. W.; Kollias, P.; Long, C. N.; Luke, E. P.; Turner, D. D.; Verlinde, J. A Focus On Mixed-Phase Clouds: The Status of Ground-Based Observational Methods. *Bull. Am. Meteorol. Soc.* **2008**, *89* (10), 1549–1562.
- (5) Vali, G.; DeMott, P. J.; Möhler, O.; Whale, T. F. Technical Note: A Proposal for Ice Nucleation Terminology. *Atmos. Chem. Phys.* **2015**, *15* (18), 10263–10270.
- (6) Després, V.; Huffman, J. A.; Burrows, S. M.; Hoose, C.; Safatov, A.; Buryak, G.; Fröhlich-Nowoisky, J.; Elbert, W.; Andreae, M.; Pöschl, U.; et al. Primary Biological Aerosol Particles in the Atmosphere: A Review. *Tellus, Ser. B* **2012**, *64* (1), 15598.
- (7) Heymsfield, A. J.; Miloshevich, L. M. Homogeneous Ice Nucleation and Supercooled Liquid Water in Orographic Wave Clouds. *J. Atmos. Sci.* 1993, 50 (15), 2335–2353.
- (8) Mitts, B. A.; Wang, X.; Lucero, D. D.; Beall, C. M.; Deane, G. B.; DeMott, P. J.; Prather, K. A. Importance of Supermicron Ice Nucleating Particles in Nascent Sea Spray. *Geophys. Res. Lett.* **2021**, 48 (3), No. e2020GL089633.
- (9) Knopf, D. A.; Alpert, P. A.; Wang, B.; Aller, J. Y. Stimulation of Ice Nucleation by Marine Diatoms. *Nat. Geosci.* 2011, 4 (2), 88–90. (10) Collins, D. B.; Zhao, D. F.; Ruppel, M. J.; Laskina, O.; Grandquist, J. R.; Modini, R. L.; Stokes, M. D.; Russell, L. M.; Bertram, T. H.; Grassian, V. H.; et al. Direct Aerosol Chemical Composition Measurements to Evaluate the Physicochemical Differences between Controlled Sea Spray Aerosol Generation Schemes. *Atmos. Meas. Technol.* 2014, 7 (11), 3667–3683.
- (11) Cochran, R. E.; Laskina, O.; Trueblood, J. V.; Estillore, A. D.; Morris, H. S.; Jayarathne, T.; Sultana, C. M.; Lee, C.; Lin, P.; Laskin, J.; et al. Molecular Diversity of Sea Spray Aerosol Particles: Impact of Ocean Biology on Particle Composition and Hygroscopicity. *Chem.* 2017, 2 (5), 655–667.
- (12) DeMott, P. J.; Hill, T. C. J.; McCluskey, C. S.; Prather, K. A.; Collins, D. B.; Sullivan, R. C.; Ruppel, M. J.; Mason, R. H.; Irish, V. E.; Lee, T.; et al. Sea Spray Aerosol as a Unique Source of Ice Nucleating Particles. *Proc. Natl. Acad. Sci. U. S. A.* **2016**, *113* (21), 5797–5803.

- (13) Gysel, M.; Weingartner, E.; Baltensperger, U. Hygroscopicity of Aerosol Particles at Low Temperatures. 2. Theoretical and Experimental Hygroscopic Properties of Laboratory Generated Aerosols. *Environ. Sci. Technol.* **2002**, *36* (1), 63–68.
- (14) DeMott, P. J.; Prenni, A. J.; Liu, X.; Kreidenweis, S. M.; Petters, M. D.; Twohy, C. H.; Richardson, M. S.; Eidhammer, T.; Rogers, D. C. Predicting Global Atmospheric Ice Nuclei Distributions and Their Impacts on Climate. *Proc. Natl. Acad. Sci. U. S. A.* **2010**, *107* (25), 11217–11222.
- (15) Martin, S. T. Phase Transitions of Aqueous Atmospheric Particles. *Chem. Rev.* **2000**, *100* (9), 3403–3453.
- (16) Estillore, A. D.; Morris, H. S.; Or, V. W.; Lee, H. D.; Alves, M. R.; Marciano, M. A.; Laskina, O.; Qin, Z.; Tivanski, A. V.; Grassian, V. H. Linking Hygroscopicity and the Surface Microstructure of Model Inorganic Salts, Simple and Complex Carbohydrates, and Authentic Sea Spray Aerosol Particles. *Phys. Chem. Chem. Phys.* **2017**, *19* (31), 21101–21111.
- (17) Morris, H. S.; Estillore, A. D.; Laskina, O.; Grassian, V. H.; Tivanski, A. V. Quantifying the Hygroscopic Growth of Individual Submicrometer Particles with Atomic Force Microscopy. *Anal. Chem.* **2016**, *88* (7), 3647–3654.
- (18) Brooks, S. D.; Wise, M. E.; Cushing, M.; Tolbert, M. A. Deliquescence Behavior of Organic/Ammonium Sulfate Aerosol. *Geophys. Res. Lett.* **2002**, 29 (19), 23-1–23-4.
- (19) Mikhailov, E.; Vlasenko, S.; Martin, S. T.; Koop, T.; Pöschl, U. Amorphous and Crystalline Aerosol Particles Interacting with Water Vapor Part 1: Microstructure, Phase Transitions, Hygroscopic Growth and Kinetic Limitations; preprint; Aerosols/Laboratory Studies/Troposphere/Chemistry (chemical composition and reactions), 2009. DOI: 10.5194/acpd-9-7333-2009.
- (20) Laskina, O.; Morris, H. S.; Grandquist, J. R.; Qin, Z.; Stone, E. A.; Tivanski, A. V.; Grassian, V. H. Size Matters in the Water Uptake and Hygroscopic Growth of Atmospherically Relevant Multicomponent Aerosol Particles. *J. Phys. Chem. A* **2015**, *119* (19), 4489–4497.
- (21) Schill, G. P.; Tolbert, M. A. Heterogeneous Ice Nucleation on Simulated Sea-Spray Aerosol Using Raman Microscopy. *J. Phys. Chem.* C 2014, 118 (50), 29234–29241.
- (22) Baustian, K. J.; Wise, M. E.; Jensen, E. J.; Schill, G. P.; Freedman, M. A.; Tolbert, M. A. State Transformations and Ice Nucleation in Amorphous (Semi-)Solid Organic Aerosol. *Atmos. Chem. Phys.* **2013**, *13* (11), 5615–5628.
- (23) Wise, M. E.; Surratt, J. D.; Curtis, D. B.; Shilling, J. E.; Tolbert, M. A. Hygroscopic Growth of Ammonium Sulfate/Dicarboxylic Acids. *J. Geophys. Res.* **2003**, DOI: 10.1029/2003JD003775.
- (24) Dawson, J. N.; Malek, K. A.; Razafindrambinina, P. N.; Raymond, T. M.; Dutcher, D. D.; Asa-Awuku, A. A.; Freedman, M. A. Direct Comparison of the Submicron Aerosol Hygroscopicity of Water-Soluble Sugars. ACS Earth Space Chem. 2020, 4 (12), 2215—2226.
- (25) Svenningsson, B.; Rissler, J.; Swietlicki, E.; Mircea, M.; Bilde, M.; Facchini, M. C.; Decesari, S.; Fuzzi, S.; Zhou, J.; Mønster, J.; et al. Hygroscopic Growth and Critical Supersaturations for Mixed Aerosol Particles of Inorganic and Organic Compounds of Atmospheric Relevance. *Atmos. Chem. Phys.* **2006**, *6* (7), 1937–1952.
- (26) Tang, M.; Chan, C. K.; Li, Y. J.; Su, H.; Ma, Q.; Wu, Z.; Zhang, G.; Wang, Z.; Ge, M.; Hu, M.; He, H.; et al. A Review of Experimental Techniques for Aerosol Hygroscopicity Studies; preprint; Aerosols/Laboratory Studies/Troposphere/Chemistry (chemical composition and reactions), 2019. DOI: 10.5194/acp-2019-398.
- (27) Lee, A. K. Y.; Ling, T. Y.; Chan, C. K. Understanding Hygroscopic Growth and Phase Transformation of Aerosols Using Single Particle Raman Spectroscopy in an Electrodynamic Balance. *Faraday Discuss.* **2008**, *137* (0), 245–263.
- (28) Yeung, M. C.; Ling, T. Y.; Chan, C. K. Effects of the Polymorphic Transformation of Glutaric Acid Particles on Their Deliquescence and Hygroscopic Properties. *J. Phys. Chem. A* **2010**, 114 (2), 898–903.

- (29) Guo, L.; Gu, W.; Peng, C.; Wang, W.; Li, Y. J.; Zong, T.; Tang, Y.; Wu, Z.; Lin, Q.; Ge, M.; et al. A Comprehensive Study of Hygroscopic Properties of Calcium- and Magnesium-Containing Salts: Implication for Hygroscopicity of Mineral Dust and Sea Salt Aerosols. *Atmos. Chem. Phys.* **2019**, *19* (4), 2115–2133.
- (30) Zamora, I. R.; Tabazadeh, A.; Golden, D. M.; Jacobson, M. Z. Hygroscopic Growth of Common Organic Aerosol Solutes, Including Humic Substances, as Derived from Water Activity Measurements. J. Geophys. Res. Atmos. 2011.
- (31) Ganbavale, G.; Marcolli, C.; Krieger, U. K.; Zuend, A.; Stratmann, G.; Peter, T. Experimental Determination of the Temperature Dependence of Water Activities for a Selection of Aqueous Organic Solutions. *Atmos. Chem. Phys.* **2014**, *14* (18), 9993–10012.
- (32) Lednev, V. N.; Grishin, M. Y.; Pershin, S. M.; Bunkin, A. F. Quantifying Raman OH-Band Spectra for Remote Water Temperature Measurements. *Opt. Lett.* **2016**, *41* (20), 4625–4628.
- (33) Suzuki, H.; Matsuzaki, Y.; Muraoka, A.; Tachikawa, M. Raman Spectroscopy of Optically Levitated Supercooled Water Droplet. *J. Chem. Phys.* **2012**, *136* (23), 234508.
- (34) Cziczo, D. J.; Abbatt, J. P. D. Infrared Observations of the Response of NaCl, MgCl₂, NH₄ HSO₄, and NH₄ NO₃ Aerosols to Changes in Relative Humidity from 298 to 238 K. *J. Phys. Chem. A* **2000**, *104* (10), 2038–2047.
- (35) Mael, L. E.; Busse, H.; Grassian, V. H. Measurements of Immersion Freezing and Heterogeneous Chemistry of Atmospherically Relevant Single Particles with Micro-Raman Spectroscopy. *Anal. Chem.* **2019**, *91* (17), 11138–11145.
- (36) Zobrist, B.; Marcolli, C.; Pedernera, D. A.; Koop, T. Do Atmospheric Aerosols Form Glasses? *Atmos. Chem. Phys.* **2008**, 8 (17), 5221–5244.
- (37) Zobrist, B.; Soonsin, V.; Luo, B. P.; Krieger, U. K.; Marcolli, C.; Peter, T.; Koop, T. Ultra-Slow Water Diffusion in Aqueous Sucrose Glasses. *Phys. Chem. Chem. Phys.* **2011**, *13* (8), 3514–3526.
- (38) Hasenecz, E. S.; Kaluarachchi, C. P.; Lee, H. D.; Tivanski, A. V.; Stone, E. A. Saccharide Transfer to Sea Spray Aerosol Enhanced by Surface Activity, Calcium, and Protein Interactions. *ACS Earth Space Chem.* **2019**, 3 (11), 2539–2548.
- (39) Maeda, M.; Lee, W. J.; Taga, N. Distribution of Lipopolysaccharide, an Indicator of Bacterial Biomass, in Subtropical Areas of the Sea. *Mar. Biol.* **1983**, *76* (3), 257–262.
- (40) Becker, S.; Tebben, J.; Coffinet, S.; Wiltshire, K.; Iversen, M. H.; Harder, T.; Hinrichs, K.-U.; Hehemann, J.-H. Laminarin Is a Major Molecule in the Marine Carbon Cycle. *Proc. Natl. Acad. Sci. U. S. A.* **2020**, *117* (12), 6599–6607.
- (41) Attard, E.; Yang, H.; Delort, A.-M.; Amato, P.; Pöschl, U.; Glaux, C.; Koop, T.; Morris, C. E. Effects of Atmospheric Conditions on Ice Nucleation Activity of *Pseudomonas. Atmos. Chem. Phys.* **2012**, 12 (22), 10667–10677.
- (42) Ladino, L. A.; Yakobi-Hancock, J. D.; Kilthau, W. P.; Mason, R. H.; Si, M.; Li, J.; Miller, L. A.; Schiller, C. L.; Huffman, J. A.; Aller, J. Y.; Abbatt, J. P. D.; et al. Addressing the Ice Nucleating Abilities of Marine Aerosol: A Combination of Deposition Mode Laboratory and Field Measurements. *Atmos. Environ.* **2016**, *132*, 1–10.
- (43) Vergara-Temprado, J.; Miltenberger, A. K.; Furtado, K.; Grosvenor, D. P.; Shipway, B. J.; Hill, A. A.; Wilkinson, J. M.; Field, P. R.; Murray, B. J.; Carslaw, K. S. Strong Control of Southern Ocean Cloud Reflectivity by Ice-Nucleating Particles. *Proc. Natl. Acad. Sci. U. S. A.* **2018**, *115* (11), 2687–2692.
- (44) Lee, C.; Dommer, A. C.; Schiffer, J. M.; Amaro, R. E.; Grassian, V. H.; Prather, K. A. Cation-Driven Lipopolysaccharide Morphological Changes Impact Heterogeneous Reactions of Nitric Acid with Sea Spray Aerosol Particles. *J. Phys. Chem. Lett.* **2021**, *12* (20), 5023–5029.
- (45) Koop, T.; Kapilashrami, A.; Molina, L. T.; Molina, M. J. Phase Transitions of Sea-Salt/Water Mixtures at Low Temperatures: Implications for Ozone Chemistry in the Polar Marine Boundary Layer. J. Geophys. Res. Atmospheres 2000, 105 (D21), 26393–26402.

- (46) Murphy, D. M.; Koop, T. Review of the Vapour Pressures of Ice and Supercooled Water for Atmospheric Applications. Q. J. R. Meteorol. Soc. 2005, 131 (608), 1539–1565.
- (47) Dick, W. D.; Saxena, P.; McMurry, P. H. Estimation of Water Uptake by Organic Compounds in Submicron Aerosols Measured during the Southeastern Aerosol and Visibility Study. *J. Geophys. Res. Atmospheres* **2000**, *105* (D1), 1471–1479.
- (48) Wang, X.; Ma, N.; Lei, T.; Größ, J.; Li, G.; Liu, F.; Meusel, H.; Mikhailov, E.; Wiedensohler, A.; Su, H. Effective Density and Hygroscopicity of Protein Particles Generated with Spray-Drying Process. J. Aerosol Sci. 2019, 137, 105441.
- (49) Zeng, G.; Kelley, J.; Kish, J. D.; Liu, Y. Temperature-Dependent Deliquescent and Efflorescent Properties of Methanesulfonate Sodium Studied by ATR-FTIR Spectroscopy. *J. Phys. Chem. A* **2014**, *118* (3), 583–591.
- (50) Wexler, A. S.; Seinfeld, J. H. Second-Generation Inorganic Aerosol Model. *Atmos. Environ., Part A* 1991, 25 (12), 2731–2748.
- (51) Jia, X.; Gu, W.; Li, Y. J.; Cheng, P.; Tang, Y.; Guo, L.; Wang, X.; Tang, M. Phase Transitions and Hygroscopic Growth of Mg(ClO₄)₂, NaClO₄, and NaClO₄·H₂O: Implications for the Stability of Aqueous Water in Hyperarid Environments on Mars and on Earth. *ACS Earth Space Chem.* **2018**, 2 (2), 159–167.
- (52) Ewing, G. E. H₂O on NaCl: From Single Molecule, to Clusters, to Monolayer, to Thin Film, to Deliquescence. In *Intermolecular Forces and Clusters II*; Wales, D. J., Ed.; Structure and Bonding; Springer-Verlag: Berlin, 2005; Vol. 116, pp 1–25.
- (53) Wise, M. E.; Martin, S. T.; Russell, L. M.; Buseck, P. R. Water Uptake by NaCl Particles Prior to Deliquescence and the Phase Rule. *Aerosol Sci. Technol.* **2008**, 42 (4), 281–294.